Journal of Magnetism and Magnetic Materials 426 (2017) 594–603

Contents lists available at ScienceDirect

Journal of Magnetism and Magnetic Materials

journal homepage: www.elsevier.com/locate/jmmm

Magnetic domains and magnetic stability of cohenite from the Morasko iron meteorite

B. Reznik[a], A. Kontny[a,*], M. Uehara[b], J. Gattacceca[b], P. Solheid[c], M. Jackson[c]

[a] Institute of Applied Geosciences, Karlsruhe Institute of Technology, Karlsruhe, Germany
[b] CNRS, Aix Marseille Univ, IRD, Coll France, CEREGE, Aix-en-Provence, France
[c] Institute for Rock Magnetism, University of Minnesota, Minneapolis, MN, USA

ARTICLE INFO

Keywords:
Morasko meteorite
Cohenite
Magnetic domains
Bitter patterns
Magnetic force microscopy (MFM)
Electron backscatter diffraction (EBSD)

ABSTRACT

Magnetic properties, texture and microstructure of cohenite grains from Morasko iron meteorite have been investigated using electron backscattered diffraction, Bitter pattern technique, magneto-optical imaging method and magnetic force microscopy. Cohenite shows much stronger magnetic contrast compared to kamacite because it is magnetically harder than the Fe-Ni alloy, and thus causes higher stray fields. A surprising result is the high stability and reversibility of the global stripe-like magnetic domain structure in cohenite when applying high magnetic fields up to 1.5 T, and exposing it to high temperatures above the Curie temperature of about 220 °C. Heating up to 700 °C under atmosphere conditions has shown that cohenite remains stable and that the global magnetic domain structures mainly recover to its preheating state. This observation suggests that magnetic domains are strongly controlled by the crystal anisotropy of cohenite. Branching magnetic domain structures at the grain boundary to kamacite can be annealed, which indicates that they are very sensitive to record deformation. EBSD observations clearly demonstrate that increasing deviation from the easy [010] crystallographic axis and stress localization are the main factors controlling the distortion of Bitter patterns, and suggest a high sensitivity of the cohenite magnetic domain structure to local microstructural heterogeneities. The results of this study substantiate the theory that cohenite can be a good recorder of magnetic fields in planetary core material.

1. Introduction

Microstructures and physico-chemical properties of iron meteorites present a window into the thermal and shock history in the early solar system (e.g [1]). Understanding of exotic magnetic phases like cohenite ([Fe, Ni, Co]$_3$C) provide a unique tool to decipher paleomagnetic signals and magnetic field records of early solar magnetic fields (e.g [2,3]). The Morasko iron meteorite, first found in 1914 near Poznan in Poland [4], contains ferromagnetic cohenite ($Fe_{2.95}Ni_{0.05}C$) [5] either along interfaces of troilite and metal [6] or as oriented inclusions in the metal following the Widmanstätten pattern [7]. The Morasko meteorite is interpreted as a product of partial melting and impact events and as such it is classified as non-magmatic IIICD [8], a subgroup of the IAB group (e.g [9,10]). Neumann lines, which are reported to result from mechanical twinning at shock pressures > 8 GPa [11] are ubiquitous (e.g [5,6]) and indicate a moderate shock metamorphic overprint.

According to Ringwood [12], the existence of cohenite indicates high pressure conditions in the meteorite. Lipschutz and Anders [13] noted that cohenite forms by exsolution from the solid state, during the cooling of an iron meteorite from 680 °C. However Brett [14] noted that cohenite indicates neither high nor low pressures but only a slow cooling in parent bodies between 650 and 610 °C. According to Wood [15] the Fe_3C stability field is large at high pressures suggesting coexistence with metallic liquid. As carbon is one of the light element candidates for the Earth's core, cohenite is suggested as a major inner core component [16]. Besides meteorites, cohenite is also described from inclusions in garnet (together with Fe-Ni and troilite) included in diamond from kimberlites [17], confirming its existence in the interior of the Earth.

The metallic ferromagnet cementite (synthetic form of natural cohenite) crystallizes in the orthorhombic structure with hexagonal close packed layers of iron with carbon filling the interstitial sites. Gao et al. [18] describes for a synthetic Fe_3C sample a magnetic transition from a low-pressure magnetic to a high-pressure non-magnetic phase above about 5.5 GPa similar to what is described for pyrrhotite [19]. Compared to all known meteorite magnetic minerals, cohenite exhibits very specific magnetic properties with a Curie temperature at 215 °C [20], which is nearly identical to the one reported for cementite about

* Corresponding author.
E-mail address: agnes.kontny@kit.edu (A. Kontny).

http://dx.doi.org/10.1016/j.jmmm.2016.10.161
Received 2 August 2016; Received in revised form 7 October 2016; Accepted 16 October 2016
Available online 08 November 2016
0304-8853/

210 °C [21]. Sugiura and Strangway [20] additionally discovered that cohenite carries the more stable component of natural remanent magnetization of the Abee meteorite (enstatite chondrite) and, therefore may be a good recorder of magnetic fields in the early solar system. Cohenite is also the main magnetic remanence carrier of lunar Apollo Mare basalt 14053 [22], suggesting that it may be an interesting mineral for lunar paleomagnetism.

Cohenite displays very prominent stripe-like magnetic Bitter patterns [6]. It is well known that the Bitter pattern method provides a quick access to the local magnetic behavior of magnetic minerals and can also be used to localize internal stress in micrograins (see e.g [23,24]). Although Bitter patterns in cohenite have been known for a long time [25], this prominent magnetic behavior was not studied in detail in relation to crystallographic orientation and microstructure of cohenite grains in iron meteorites. Magnetic force microscopy (MFM) combined with electron backscattered diffraction (EBSD) measurements of globular cementite embedded in a ferrite matrix is reported in a metallurgical study of Batista et al. [26]. These authors found that the easy direction of magnetization in the orthorhombic cementite is the long [010] axis (a=5.09 Å, b=6.74 Å, c=4.52 Å). According to measurements of the saturation magnetization and crystallographic anisotropy of cementite as a function of temperature Blum and Pauthenet [27] suggested that the [001] axis is the easy axis of magnetization (which, in this case, is also the long axis of the unit cell). In uniaxial materials like the orthorhombic cementite/cohenite one axis is favored over the other two (hard) axis, which produce a strong anisotropy in these crystals. Blum and Pauthenet [27] report that cementite is a relatively hard magnetic material with high single crystal anisotropy constants (K_1=118×10^3 Jm^{-3} and K_2 =394×10^3 Jm^{-3}). Thus [010] is the easiest and [100] the hardest direction of magnetization. In terms of the nomenclature used in Batista et al. [26] and in our study, this corresponds to the b and a axis, respectively. To date, no information is available on the magnetic and thermal stability of the magnetic structure of natural cohenite.

We present in our study Bitter pattern, magneto-optical imaging (MOI) and magnetic force microscopy (MFM) results of cohenite from the Morasko meteorite and correlate this information with the crystallographic orientation and internal stress determined by EBSD measurements. The effect of an external laboratory magnetic field on the magnetic domain structure is studied using the MOI technique [28,29]. In order to understand the strong magnetic stability of cohenite we combined thermomagnetic measurements from room temperature to above the Curie transition with Bitter pattern and magnetic force microscopy imaging.

2. Sample description and analytical techniques

A description of the different phases of Morasko iron meteorite and their mineralogical composition is reported in detail elsewhere [6]. Briefly, it consists of a Fe-Ni alloy matrix (about 98 vol%) and troilite (FeS) nodules occupying about 2 vol%. The matrix is mainly composed of kamacite with α-Fe cell and less than 6% of Ni, and taenite with γ-Fe-cell and more than 20% Ni. Accessory minerals, mostly occurring in the margins of the troilite nodules, are schreibersite ($[Fe, Ni]_3P$), cohenite ($[Fe, Ni, Co]_3C$), sphalerite (ZnS), graphite (C), daubreelite ($FeCr_2S_4$) and silicate minerals (Na-pyroxene and plagioclase) [6]. Similarly to its metallurgical analogue cementite (Fe_3C), cohenite exhibits extraordinary corrosion/etching resistance and exceptionally high hardness. As a result, cohenite can be easy distinguished from schreibersite, kamacite, and taenite on polished surfaces [25].

Using a diamond saw, the sample from the interfacial area was cut in form of a small slab, embedded into epoxy resin and polished using diamond and alumina pastes. Optical microscopy (Leica Orthoplan microscope coupled with a Leica DFC 420C CCD camera) in reflected light was used to study the magnetic domain structure (uniformly magnetized region) using Bitter pattern technique. This technique is useful as it is sensitive to small variation in magnetization. For this purpose, the polished surfaces were coated with ferrofluid (EMG 807, Ferrofluidics GmbH) diluted with distilled water in the ratio 1:10.

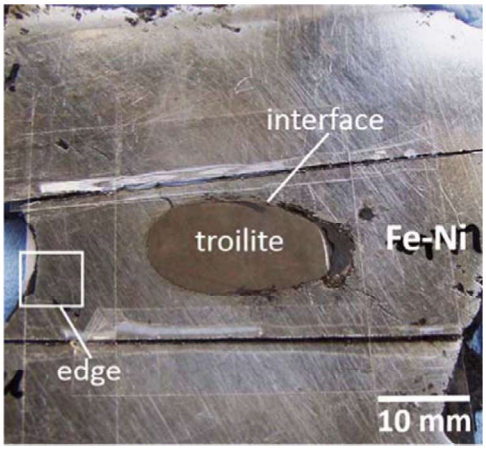

Fig. 1. An optical micrograph of the studied meteorite piece composed of troilite nodule surrounded by a Fe-Ni alloy. Two areas of interest are labeled - the interface and edge. (For interpretation of the references to color in this figure legend, the reader is referred to the web version of this article.)

The crystallographic texture was studied by electron backscattered diffraction (EBSD) using a Zeiss EVO MA 10 scanning electron microscope (SEM) (Zeiss AG, Germany) equipped with an EBSD pattern detecting system and the ESPRIT software (Bruker Nano GmbH, Germany) for data handling and analysis. The acceleration voltage was 20 kV, and probe current was 6 nA. The working distance between specimen and electron gun was 14 mm, and between specimen and EBSD detector it was 17 mm.

The effect of an external magnetic field on the magnetic domain structure of cohenite was investigated using magneto-optical (MO) imaging technique utilizing a Leica DM2500P microscope and a low-noise black and white CCD camera (Ikon-M, Andor Technology), as described in detail in previous studies [28,29]. The acquired MO images correspond to a saturation isothermal remanent magnetization state formed after applying a strong magnetic field (1.5 T). The magnetic field was imparted with a MMPM-9 (Magnetic Measurements Ltd.) pulse magnetizer.

Magnetic susceptibility as a function of temperature around the Curie transition of cohenite (~220 °C) was measured using an AGICO KLY-4S kappabridge (effective field intensity:300 A/m; frequency:=875 Hz). In order to reveal the effect of temperature cycles on the evolution of magnetic structures, a mini sample (about 2.5×2.5×4.5 mm^3) containing high concentration of cohenite was cut from the meteorite using a diamond saw. Before and after temperature cycling, the polished sample surface coated with ferrofluid was studied with an optical microscope. The heating-cooling cycles were done in an argon atmosphere (flow rate of 110 mL min^{-1}) with a heating rate of 11°min^{-1}. The Curie temperature was calculated from the minimum in the first derivative curves while the transition width corresponds to the full width at half maximum (FWHM) of the derivative curves.

In-situ high-temperature observation of the magnetic domain structures was done using an Asylum Research MFP-3D magnetic force microscope (MFM). The MFM cantilevers are made from silicon or silicon nitride coated with CoCr. The MFP-3D collects high-pixel-density images (up to 5k×5k) with high-speed data capture up to 5 MHz. The heating-cooling runs around the Curie point of cohenite were done in air using temperature interval varying from 20 to 50 °C. The temperature was maintained to better than 0.2 °C precision with accuracy to 0.5 °C and temperature overshoots less than 0.2 °C.

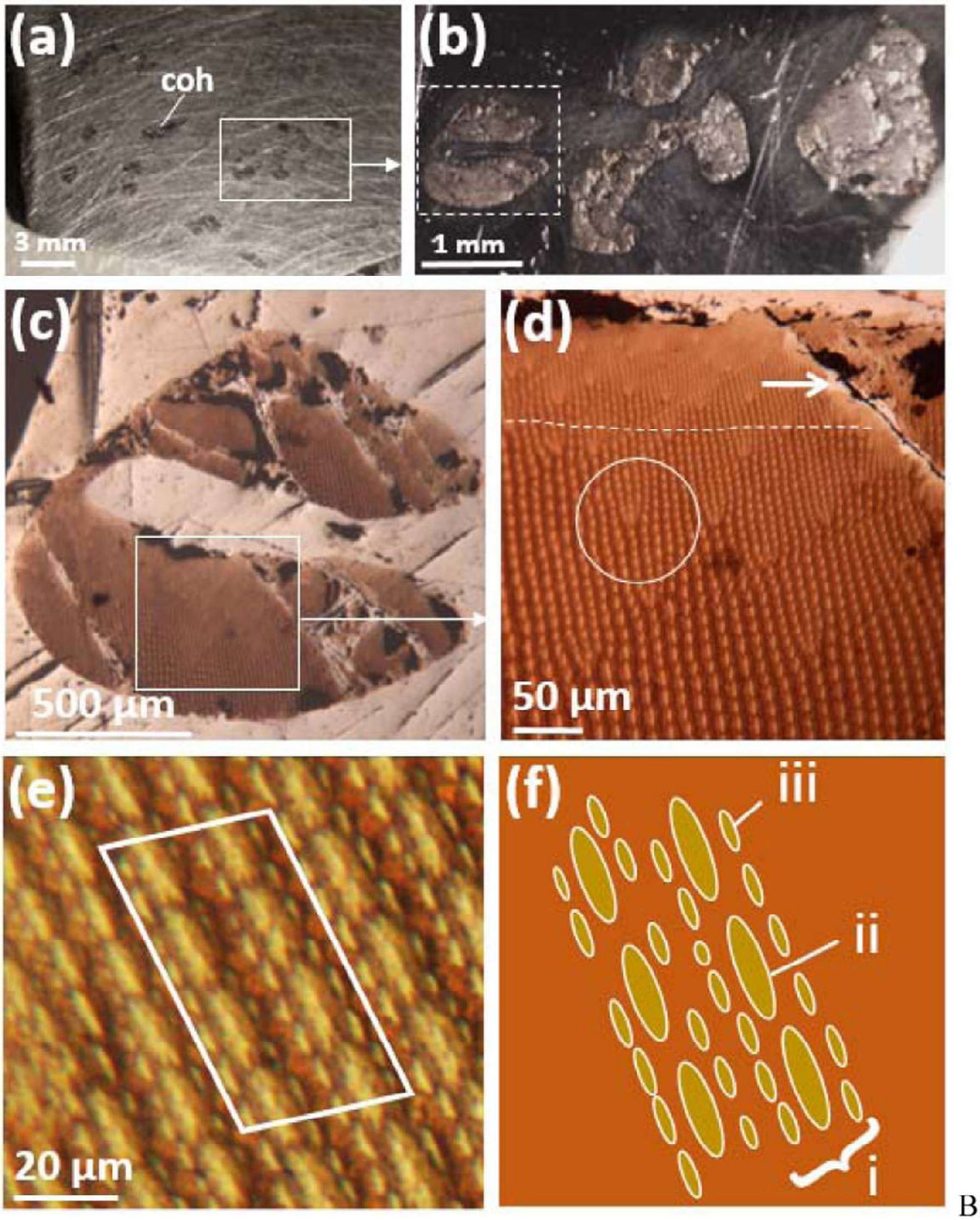

Fig. 2. Morphology and magnetic domain structure of cohenite grains from the edge region, shown in box from Fig. 1. (a) Roughly polished area enriched with mm-sized cohenite grains (dark grey) revealed by ferrofluid; (b) Magnified region from (a) containing globular-shaped grains; (c) Magnetic domain structure revealed by Bitter pattern method in a well-polished cohenite grain (s. the dashed box in (b)); (d) Enlarged central part of the area labeled by the box in (c). The horizontal dashed line is an approximate margin between areas containing low (bottom) and high concentration (top) of branched micromagnetic structures. The arrow points to a weak magnetic contrast near the crack; (e) Hierarchical system of micromagnetic structures (enlarged bottom part containing no branched bands from (d)) on a surface plane tilted in an angle of about 30° from the easy axis direction [010] (see Fig. 4a); (f) Schematic illustration of the area labeled by the parallelogram in (e) showing primary structures (i) composed of elongated islands (ii) as secondary structures, and satellites (iii) as ternary structures. (For interpretation of the references to color in this figure legend, the reader is referred to the web version of this article.)

3. Results

3.1. Magnetic domain structures observed by Bitter pattern

The studied meteorite piece is composed of a rounded troilite nodule enclosed in a Fe-Ni alloy matrix (Fig. 1). Relative to the nodule location, samples from the troilite-alloy interfacial area and from the edge area located at some distance from the interface within the Fe-Ni alloy were studied. As it can be recognized in the optical micrograph of Fig. 1, the surface of the studied meteorite piece is roughly pre-polished. When the piece is covered with a ferrofluid agent, numerous mm-sized cohenite grains can be recognized even using folding lenses

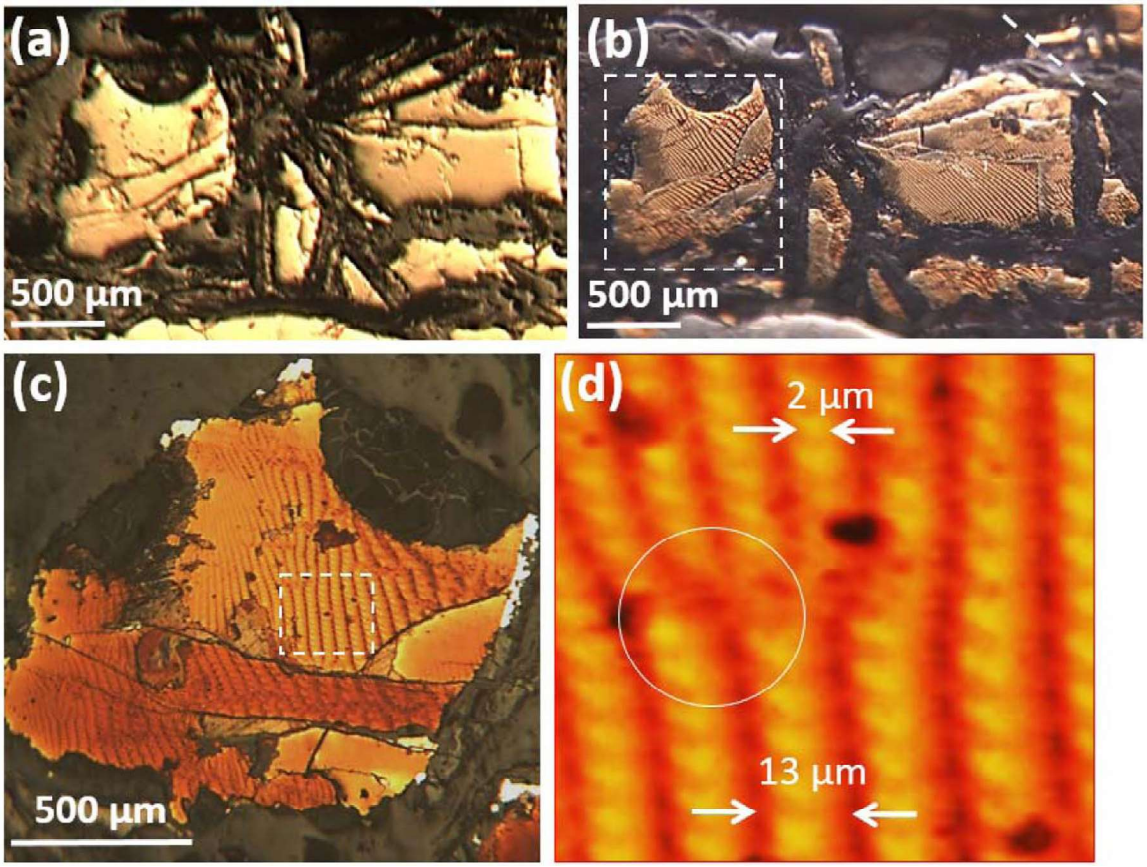

Fig. 3. Morphology and magnetic domain structure of cohenite grains from the troilite-alloy interface (see also Fig. 1). (a) Cohenite grains observed after 1 min etching with nital. (b) The same area as in (a) but covered with ferrofluid. Note that in different grains the Bitter patterns exhibit similar global texture indicated by the white dashed line; (c) Magnified image of the grain labeled by the box in (b) shows that some subgrains do not show Bitter patterns; (d) Enlarged central part of the grain from (c) showing 13 µm wide periodic bands, 2 µm-sized islands and dislocation-like branched structures (see e.g. the circled area). Note that compared to the sample from the edge area (Fig. 2e, f) the ternary structures with satellites are less developed. (For interpretation of the references to color in this figure legend, the reader is referred to the web version of this article.)

(Fig. 2a). Frequently, the cohenite grains exhibit a conspicuous flexuous globular-shaped morphology (Fig. 2b).

After polishing, well-developed striped Bitter patterns with bright dots in a dark (brown) matrix are observed (Fig. 2c–e), typical for anisotropic uniaxial material. This bright and dark pattern is related to the micromagnetic structure at the sample surface and the resulting stray-field distribution. It corresponds to components of magnetization out of and into the plane of the image. It is important to note that the same magnetic texture and orientation was observed in all grains located within the edge area. The local character of Bitter patterns is however different. Relatively straight, partly branching walls are typical for the bottom parts of the grain in Fig. 2d. In the upper part of the grains, the density of the branching subdivisions is significantly higher (see e.g. the region laying above the dashed line in Fig. 2d) suggesting higher internal stresses in the cohenite crystal towards this grain boundary. Furthermore, the patterns frequently disappear in the vicinity of cracks (see e.g. the area labeled by arrow in Fig. 2d). At a higher magnification, the magnetic microstructure is hierarchical (Fig. 2e) and can be represented as a system of different micromagnetic structural units (Fig. 2f). The primary structure *i* with a periodic distance of about 10 µm corresponds to the dark bands, the secondary structure *ii* is related to elongated islands with lengths from 2–8 µm, while the ternary structure *iii* corresponds to fine satellites (Fig. 2f) with lengths lying below 2 µm.

Fig. 3 shows representative optical micrographs of cohenite grains located at the troilite-alloy interface shown in Fig. 1. In this sample, grains composed of µm-sized cohenite (up to a size of about 50 µm) in association with schreibersite, troilite and carbon are observed (Fig. 3a). Cohenite grains again show striped Bitter patterns (Fig. 3b). Due to a subdivision of the grains by cracks into subgrains they exhibit now heterogeneous magnetic contrasts (Fig. 3c) and the stripes are not exactly parallel. For example, in the central part of the grain shown in Fig. 3c the primary domain structure appears in form of alternating bands containing dislocation-like, branched configuration (white circle in Fig. 3d). The average periodic distance between bands is about 13 µm. Each band is composed of elongated islands having a width of 2 µm. Compared to the cohenite inclusions in the alloy (Fig. 2e and f), the satellites cannot be recognized in cohenite grains from this area. Furthermore, this area is also characterized by a larger amount of magnetic subgrains exhibiting no Bitter pattern (Fig. 3c). This fact suggests that the crystal orientation and the presence of local structural distortions have a significant influence on the domain structure and therefore it was studied in detail by EBSD (Fig. 4).

3.2. Texture analysis by EBSD

Fig. 4a and b show EBSD pole and inverse pole figures (IPF) for the edge and interface area, where the sample surface Z direction is parallel to the electron beam. The cohenite grains from the edge area are tilted in an angle of about 30° from the easy [010] axis (Fig. 4a). The grain normals are approximately coincident with the [101] direction (Fig. 4a, inset). Compared to the edge area, the grains from the interface area exhibit larger (near 45°) deviation from the magnetic easy axis (Fig. 4b). This increasing deviation angle between the normal to the surface plane and the easy [010] axis explains the difference in magnetic domain pattern, with its more dot-like appearance in the edge area (Fig. 2) and the more stripe-like one in the interface area (Fig. 3). According to the IPF data (Fig. 4b, inset), the normals of the

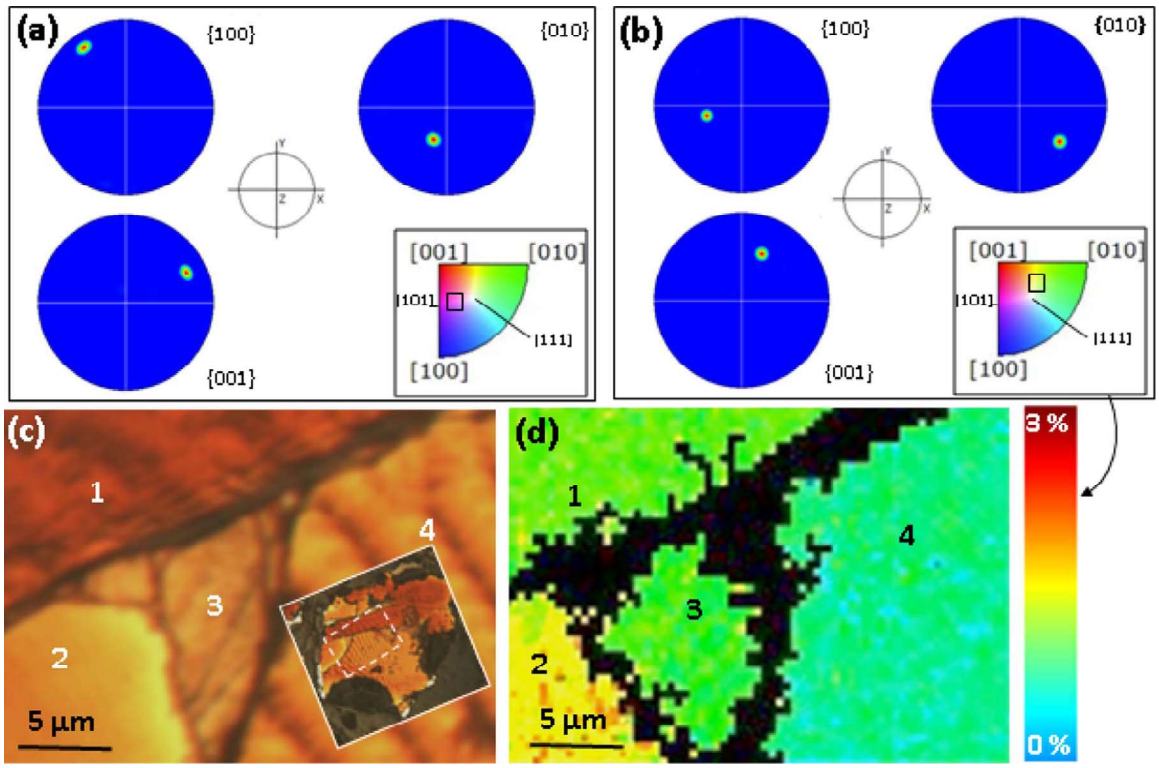

Fig. 4. EBSD analysis of cohenite grains. (a) Pole figures and an inverse pole figure (inset, right bottom) related to the edge area. (b) Pole figures and an inverse pole figure (inset, right bottom) related to the interface area. (c) Bitter patterns in a grain (the enlarged area labeled by the dashed box in inset) from the interface area (see also Fig. 3c). Note the different magnetic contrast in subgrains 1, 2, 3 and 4; (d) Misorientation EBSD map across the subgrains shown in (c). The inverse pole figures are plotted with respect to the sample normal direction. The black boxes in inverse pole figures symbolize the orientation of the grain lying approximately perpendicular to the electron beam. (For interpretation of the references to color in this figure legend, the reader is referred to the web version of this article.)

interfacial grains occupy an intermediate position lying between [111] and [010] directions.

In the subgrains with different magnetic contrast (Fig. 4c), small but detectable deviations of the crystallographic orientation is illustrated by the corresponding misorientation map (Fig. 4d). Illustrated by the vertical colored strip scale in Fig. 4d, the relative lattice distortions lie in a narrow range spreading from 0% to 3%. The highest misorientation of about 1.5% (yellow dots) is measured within subgrain 2 exhibiting no visible Bitter pattern as well as at vicinities of cracks running around the subgrains 1, 3 and 4. The mosaic areas displaying the lowest misorientation degree approaching 0% (blue dots) are localized within subgrain 4. In summary, the results obtained by a combination of the Bitter pattern method and EBSD clearly demonstrate an amazing high sensitivity of the cohenite magnetic structure to local misorientation, which especially developed within the interfacial troilite-metal area. Cohenite from this area shows a multitude of intragranular cracks, microfractures and branched Bitter patterns (Fig. 3), which are less pronounced in the edge area (Fig. 2).

3.3. *Magneto-optical imaging of remanent magnetic structures*

In order to gain information on the magnetic stability of magnetic domains in cohenite magnetic field experiments of a sample saturated at 1.5 T were combined with the magneto-optical (MO) imaging technique (Figs. 5 and 6). This technique maps the stray field of the magnetization (artificial or natural) of a polished sample [28]. The initial, natural magnetization state is characterized by a well-contrasted MO image (Fig. 5a) displaying 180° basic stripe-shaped domain walls with a strong magnetic contrast and a complex branched pattern in appearance similar to those observed by the Bitter pattern method (Fig. 2c–e). To achieve a first magnetic saturation state, the sample was imparted a saturation isothermal remanent magnetization (SIRM) by exposure to 1.5 T field oriented perpendicular to the sample surface and oriented away from the polished surface (Fig. 5b). Images were then taken in zero field. Besides cohenite, an elongated taenite grain can now be recognized inside the kamacite matrix by its strong magnetic signal. The resulting domain pattern in cohenite changes from stripe-shaped to mesh-shaped arrays containing interconnected thinner units (see inset in Fig. 5b). It is interesting to note that the microstructural sample heterogeneity of the initial state is adopted. Large elongated domains are formed within areas containing a low density of branched patterns while the small meshes are formed in areas having enhanced density of the branched patterns (compare with Fig. 2d). Using −50 mT backfield demagnetization steps in opposite direction (perpendicular and oriented into the polished surface), changes in domain structure development became visible at about −400 mT (Fig. 5c and d). This observation suggests a quite hard magnetic behavior of cohenite. The −400 mT state is characterized by a breakdown of the closure domains (Fig. 5d). With further increasing field to −1.5 T closure domains in combination with a magnetic moment flip develop again (Fig. 5e and f). In this state, the magnetic domains are nearly inverted (Fig. 5f) with respect to Fig. 5b, in agreement with a switched magnetic field.

Applying again a 1.5 T magnetic field perpendicular and out of the plane of the polished surface, the closure domains appear again (Fig. 6a) and are very similar to the domain pattern formed after the first magnetic field application (Fig. 5b). This observation indicates a good magnetic reversibility of the cohenite magnetic domain structure. Also similar to the first run (Fig. 5d), the closure domains disappear at a field of about −300 mT (Fig. 6b) and stripe domains form again (Fig. 6c). More stripe-like domains also form when applying an in-plane field of 1. 5 T oriented parallel to the global magnetic texture (Fig. 6d). This magnetic structure can be transformed again into the closure-domain structure when the applied in-plane 1.5 T field is oriented perpendicular to the global magnetic texture (Fig. 6e and f). It can be easily seen that the structure shown in Fig. 6e is nearly

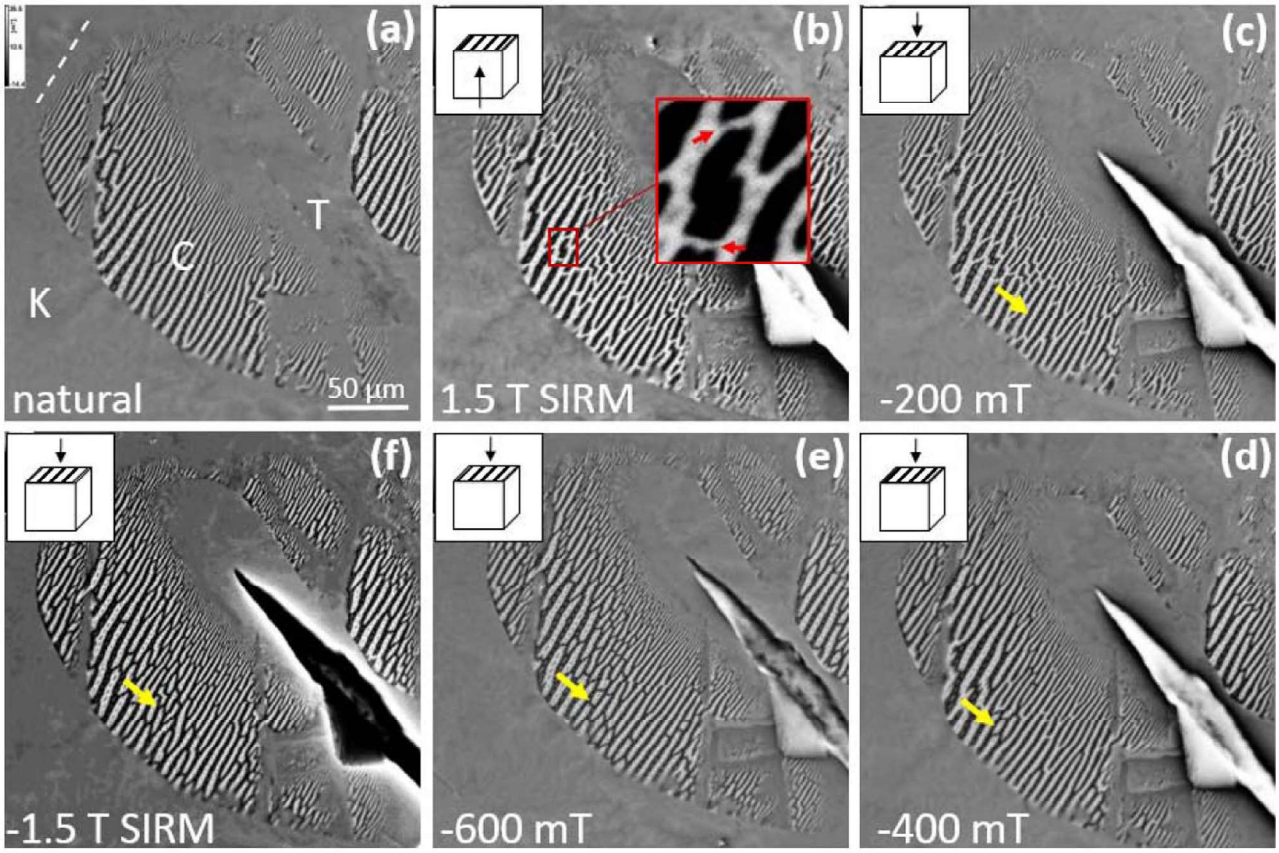

Fig. 5. Magneto-optical images of magnetic domains in a cohenite grain from the edge region (same grain as in Fig. 2c) before and after given a saturation isothermal remanent magnetization (SIRM) at 1.5 T out of the plane followed by successive back-field demagnetization steps (from (c) to (f)) in the opposite direction (into the plane). All images are taken in zero field after switching off the field. The whitish (blackish) grayscale corresponds to the upward (downward) surface magnetic field. (a) Stripe-like pattern with partly branched regions in the natural state (compare Fig. 2c and d). The dashed line indicates the initial global domain texture. Kamacite, cohenite and taenite are labeled by K, C and T, respectively; (b) and (c) Development of mesh-shaped arrays (see e.g. the inset in (b)); (d) and (e) Development of broken walls (see e.g. the arrow in (d)); (f) Formation of an oblong structure exhibiting inverse contrast with respect to the state shown in (b). The magnetic field vector in (b)–(f) is perpendicular to the image plane and in a steep angle with the easy magnetic axis [010] of cohenite. The scale bar shown in (a) is the same for all images. (For interpretation of the references to color in this figure legend, the reader is referred to the web version of this article.)

inverted with respect to the structure shown in Fig. 6d and is similar to the first run (Fig. 5b and f).

3.4. Temperature-dependent magnetic susceptibility and magnetic domains revealed by Bitter pattern

In earlier experiments from the troilite-alloy interface area of the Morasko iron meteorite a peak at 176 °C was observed in the temperature-dependent magnetic susceptibility curve, which was interpreted as Curie temperature (T_C) of cohenite [6]. This transition temperature vanished during a heating-cooling cycle up to 700 °C. Therefore in our new study, we heated a polished piece from the edge area (Fig. 1) to maximum temperatures of 230 and 250 °C, respectively, in the furnace of our kappabridge. In a first heating-cooling cycle a relatively sharp T_C around 220 °C was observed (Fig. 7), which is in good agreement with literature data of T_C of cohenite [31]. During this first heating, an increase in magnetic susceptibility was observed until about 160 °C, while during cooling magnetic susceptibility roughly remains constant below T_C. A second heating-cooling cycle revealed a better reversibility and a slight increase of the magnetic susceptibility (red curves in Fig. 7).

Before (a) and after the first (b) and second (c) temperature cycling the Bitter pattern of the polished surface was studied (Fig. 8). Initial magnetic domains are characterized by well-resolved stripes containing branched regions, which are especially developed at the cohenite-Fe-Ni alloy interface (see circles in Fig. 8a). Similarly to the case presented in Fig. 2e, islands and satellites are clearly detectable at a high magnification (s. inset in Fig. 8a). After the first heating-cooling cycle (Fig. 7) some of the branched regions disappeared (see branched region inside dashed circle in Fig. 8a and b). Furthermore, it appears that the islands and satellites become broader and sharper, and much smaller details are visible inside of islands and satellites (inset in Fig. 8b).

After the second heating-cooling cycle (Fig. 8c), some of the branched bands disappear (see bold circle in Fig. 8c) but simultaneously some branched bands appear again (see dashed circle). At higher magnification, islands and satellites became thinner and the number of satellites increases (s. inset in Fig. 8c). Now, a big number of islands are fused together forming ribbon-shaped domains (s. red arrow in inset of Fig. 8c).

3.5. In-situ high-temperature magnetic domain observation from magnetic force microscopy

Using a magnetic force microscope (MFM) with a heating stage, we investigated the evolution of magnetic domains during heating above the T_C and cooling back to room temperature. MFM images the magnetic force gradient due to the stray field from the surface of a sample. MFM images were taken close to the area labeled in Fig. 2c. Compared to the Bitter pattern (Fig. 2c) and MO imaging (Figs. 5 and 6), MFM images provide significantly more detailed information on magnetic domains (Fig. 9a). Small islands have been already resolved within the black and white stripes of the MO images (e.g. Fig. 6c and f) but in MFM images they are more complex and show up on different scales. The stripes are full of closure domains now, which cause a more

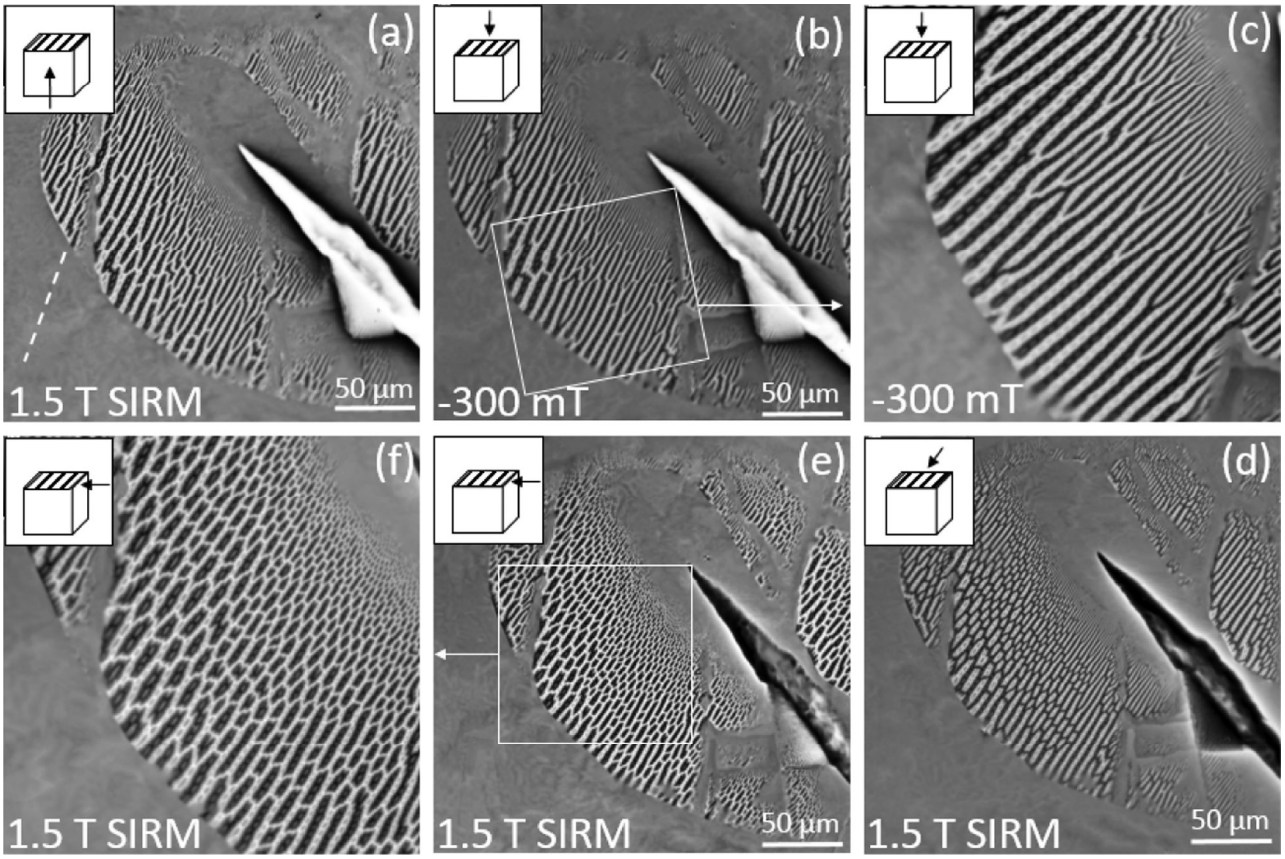

Fig. 6. Magneto-optical images of magnetic domains in cohenite from the edge region (see grain shown in Fig. 2) as function of the orientation of the applied magnetic field (H). All images are taken in zero field after switching off the field. (a) Closure domains with similar features as shown in Fig. 6b. Dashed line indicates the global domain texture. (b) and (c) shows the partly disappearance of closure domains and formation of stripe-like domains. (c) Enlarged view from area indicated by white rectangle in (b); (c) and (d) Formation of pronounced oblong closure domains; (e) and (f) Formation of pronounced closure domains being inverted with respect to (d). (f) Enlarged view from area indicated by white rectangle in (e). Magnetic field vector is perpendicular to the image plane in (a–c), parallel to the global domain texture in (d), and perpendicular to the global domain texture in (e) and (f). The image planes are nearly coincident with the [101]-axis of cohenite.

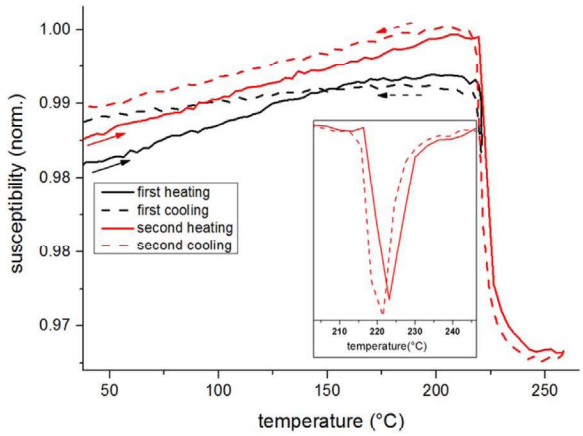

Fig. 7. Magnetic susceptibility as a function of temperature measured in two successive heating-cooling cycles (black and red curves) in argon atmosphere. Inset shows first derivatives around the Curie point. Note the increasing reversibility in susceptibility during the second run (red curves). (For interpretation of the references to color in this figure legend, the reader is referred to the web version of this article.)

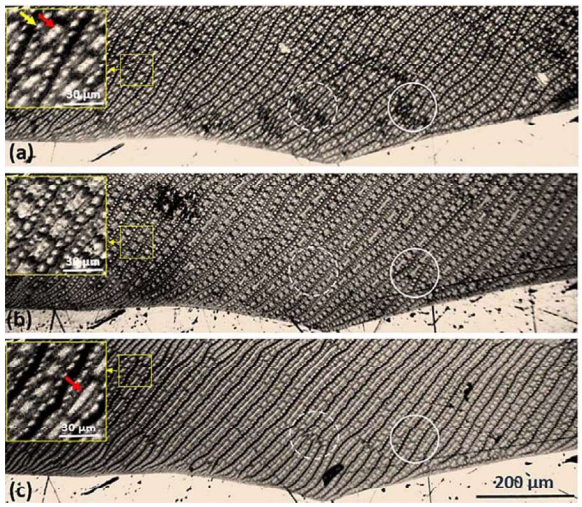

Fig. 8. Magnetic domain structures revealed by Bitter pattern method before (a) and after (b, c) two successive susceptibility measurements shown in Fig. 7. (a) Initial state. Elongated bands containing branched regions (see e.g. two areas labeled by circles). Islands and satellites are shown in inset by red and yellow arrow, respectively. (b) After first heating-cooling cycle. Some of branched bands disappear (see e.g. the area within the dashed circle). Islands and satellites increase in size (inset). (c) After second heating-cooling cycle. Some of branched bands disappear (see e.g. the area within the bold circle) while others reappear (see e.g. the area within the dashed circle as well as the areas located at the cohenite-kamacite interface at the left side). Inset: islands and satellites became thinner and the number of satellites increases. Some islands are fused into ribbons (arrow). (For interpretation of the references to color in this figure legend, the reader is referred to the web version of this article.)

blurred appearance within the white and black stripes.

After each increase in temperature it was necessary to withdraw and re-tune the MFM cantilever because the resonant frequency changes with temperature. Due to minor drift of the cantilever position, it re-engaged the surface at a slightly different position each time, so the image areas in Fig. 9 do not match up exactly. The arrows indicate a fixed location in the image set. Heating up to the Curie point of 220 °C

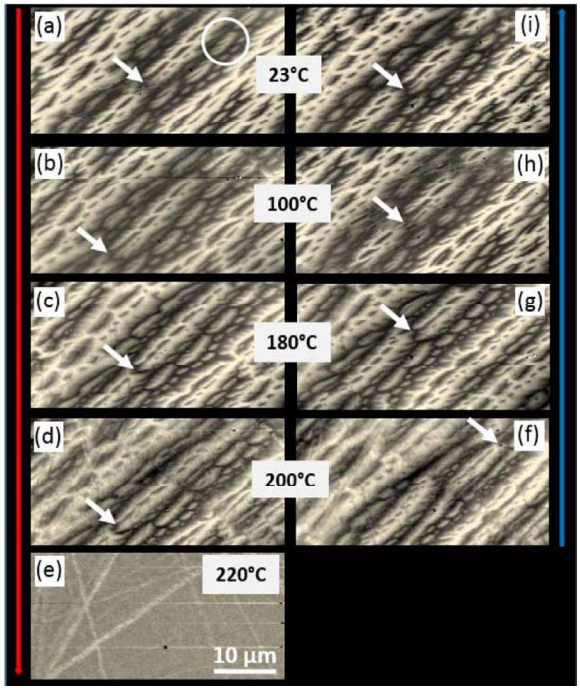

Fig. 9. MFM imaging of magnetic domains in cohenite as a function of temperature at atmosphere conditions. A cluster containing islands and satellites is labeled by the white circle in (a). The arrows mark the localization of the same specific branched feature. No magnetic domains occur above the Curie temperature in (e) indicating the paramagnetic state. The image planes are in a steep angle to the easy [010] axis of cohenite (compare with Fig. 4a). Scale bar shown in (e) is the same for all images. Heating and cooling were done in ambient field conditions in the MFM (~0.25 mT), so the final state in (i) is a 250-microtesla thermal remanent magnetization. (For interpretation of the references to color in this figure legend, the reader is referred to the web version of this article.)

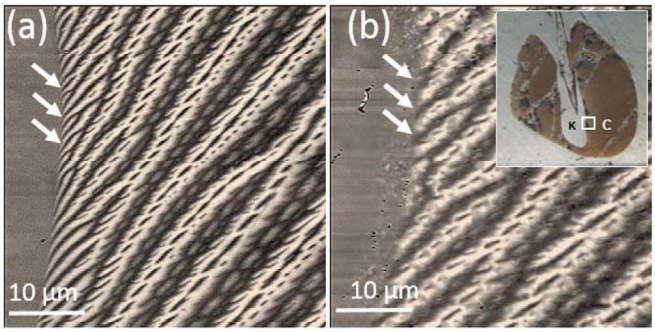

Fig. 10. MFM imaging of a cohenite-kamacite interface (a) before and (b) after heating to 700 °C under atmosphere conditions. Branching of magnetic domains (e.g. see arrows) toward the kamacite (left) disappears after heating and grain boundary migrates into the cohenite grain. The studied area is shown by the white box in the inset in (b). The image planes are nearly consistent with the [101] axis of cohenite. (For interpretation of the references to color in this figure legend, the reader is referred to the web version of this article.)

(e) a successive coarsening and a partial disappearance of bands, islands and satellites is observed. At a temperature of 220 °C the magnetic domains are no longer visible indicating paramagnetic behavior (e). During cooling (Fig. 9f–i), a reversible recovery with higher contrasts of the magnetic microstructures occurs. Compared to the initial state (a) the islands and satellites are finer after the cooling (i). MFM data clearly demonstrate a good thermal reversibility of cohenite magnetic domains under atmosphere conditions. This high reversibility of magnetic domains is even observable when the sample is heated under atmosphere conditions to 700 °C (Fig. 10). The global magnetic domain structure is still very similar, but the branched region at the grain boundary to kamacite has been removed. This behavior clearly verify that the branching indicate higher internal stresses towards the grain boundary, because they can be annealed by temperature.

4. Discussion and conclusions

In this study we present a relationship between magnetic properties, texture and microstructure of mm-sized cohenite inclusions in Fe-Ni alloy from the Morasko meteorite, Poland. Strong magnetic contrasts are found with all three magnetic domain imaging techniques: Bitter pattern, magneto-optical and magnetic force microscopy. In contrast to kamacite, cohenite shows much stronger magnetic contrast because it is magnetically harder than the Fe-Ni alloy, and thus causes higher stray fields. The [010] easy axis of magnetization lies at a moderately high angle to the image plane, and there is therefore a strong out-of-plane component of magnetization in all of the images. The [001] hard axis of magnetization is approximately perpendicular to the alternately magnetized parallel stripes (Fig. 4a). The most surprising result is the high stability and reversibility of the global stripe-like magnetic domain structure when applying high magnetic fields up to 1.5 T, and exposing it to high temperatures above the Curie temperature of about 220 °C and up to 700 °C. This observation is surprising because graphite is the stable form of C at low pressure and temperature (< ca. 630 °C [7]) and cohenite is assumed to be metastable in iron meteorites.

Heating up to 700 °C under atmosphere conditions revealed that cohenite remains stable and that the global magnetic domain structures mainly recover to its preheating state (Fig. 10), but branching domain structures at the grain boundary to kamacite can be annealed. This observation indicates that while the main domain pattern is controlled by the magnetocrystalline anisotropy, the branching of the domains is additionally controlled by stress and magnetoelastic anisotropy and is very sensitive for deformation of cohenite. Similar high sensitivity of branching structures to record deformation is recently clearly demonstrated in magnetic domains of Fe-3%Si [32]. We also discovered that the magnetic domain structure is significantly different in the two investigated areas with well-aligned domain walls in cohenite embedded in the metal (Fig. 2), while grains with a higher concentration of microcracks at the troilite - metal interface (Fig. 3) show a more disturbed pattern. This observation suggests a more elastic deformation of cohenite in the metal and a more brittle deformation at the metal-troilite interface. EBSD observations (Fig. 4) clearly demonstrate that the stress localization is a main factor controlling the distortion of Bitter patters, and suggest a high sensitivity of the cohenite magnetic domain structure to local microstructural heterogeneities.

In general, magnetic domains are formed to minimize the total energy of the magnetic mineral, and stray field energy is an important part of it. Different magnetic imaging techniques allowed us to study different behavior of magnetic domains in cohenite. The Bitter pattern method provides an easy and quick access into imaging of magnetic domains over a broad structural range from micrometers to several millimeters (Figs. 2 and 7). The derived image contrast and resolution are however especially sensitive to the sample surface quality controlling spreading of liquid ferrofluid. Therefore, the Bitter pattern method is not very operative for dynamic investigations, particularly at elevated temperatures. For the high-temperature dynamic imaging of magnetic domains MFM is an irreplaceable tool (Figs. 9 and 10). Moreover, magneto-structural details on a micrometer scale can be observed (see e.g. satellites in Fig. 9). Compared to the Bitter pattern method, MFM allows analyzing relatively small sample areas, which maximal size is about 100*100 μm^2, but this method is extremely sensitive to the surface quality. Compared to MFM and Bitter pattern method, MOI provides an exclusive access to investigate the dynamics of magnetic domains on a broad optical scale (Figs. 5 and 6). Moreover, this method is not very sensitive to the sample surface quality.

Our magnetic field experiments connected with MOI imaging

revealed significant aspects of the magnetic behavior of cohenite:

1) The magnetic structure starts to change irreversibly when the external magnetic field is more than 200–300 mT, indicating a very high coercivity of remanence (Figs. 5 and 6). This observation is not in agreement with Batista et al. [26] who reported a change in magnetic domain wall configuration in ca. 3 μm sized globular cementite grains (the synthetic analogue of natural cohenite) embedded in steel already in external magnetic fields of 22,000 A/m (27.6 mT), which is one magnitude lower than in our observations. This discrepancy is probably related to the different methodological approaches: in our experiment the images were taken after switching off the field, whereas Batista et al. [26] observed induced magnetization.
2) The local structural heterogeneity in form of areas containing high concentration of branched structures is very stable even after a strong 1.5 T field is applied and removed. Therefore basic magnetic domains in cohenite seem to be very stable. Branched magnetic domains, indicating internal stress in the lattice, can however be removed by heating the sample up to 700 °C (Fig. 10b).
3) The change of magnetic domain pattern from stripes to mesh-shaped arrays within the basic stripes is caused by the minimization of stray field energy in an external magnetic field.
4) Independent of external magnetic field direction (in and out of plane, parallel and perpendicular to global magnetic domain structure along the surface) the magnetic contrast remains strong, indicating that magnetic moments remain vertically arranged after the field of 1.5 T is removed. Either magnetocrystalline anisotropy or magnetostriction can be sufficient to cause large out-of-plane magnetization components [24]. The observed satellites (Figs. 8 and 9) look similar to the "spike domains" discovered by Moskowitz et al. [33] in synthetic Ti-rich titanomagnetite. These authors explained this observation by a strong uniaxial stress anisotropy, which overwhelms the cubic crystallographic anisotropy in the stressed surface layer.

Keh and Johnson [31] reported already that the strip-shaped domains in cementite are alternately magnetized along the positive and negative direction of the easy axis of magnetization. According to Batista et al. [26] magnetic domain pattern in μm-sized (~3 μm) cementite inclusions are also formed along the long [010] easy direction of magnetization. These authors also noted an important relationship between MFM and EBSD data (for details see Fig. 6 in [26] and its corresponding description): some of the cementite inclusions are mainly oriented around the (010) plane while the domain structure of most of the precipitates consists of parallel stripes, and no closure domains are observed. These observations correlate very well with our data showing well-resolved stripe-shaped domains with alternating magnetic contrast (Figs. 2–4) oriented in a moderate to steep angle to the easy axis of magnetization [010] and approximately perpendicular to the hard axis of magnetization [001]. In perpendicular view to the surface shown in Fig. 2, we also observed alternating sharp magnetic stripe domains (not shown) and therefore the best explanation we can suggest is that stripe-like magnetic domains occur in a large range of angles between surface planes and easy magnetic axis. More detailed investigations are needed in future to better characterize and understand this phenomenon. Furthermore, we found out that a small misorientation above about 1.5% from the crystallographic axis is sufficient to erase the prominent stripe-like magnetic domain pattern indicating the sensitivity of the magnetic domains in relation to the crystallographic axis. The sensitivity for brittle deformation and stress-induced deformation in the lattice becomes especially obvious in cohenite from the interface area (Figs. 1 and 3).

The contribution of cohenite to the magnetic properties and crystallization conditions of extraterrestrial material is not well constrained although some references are given. Sugiura and Strangway [20] reported for the first time that the stable part of the natural remanent magnetization of the Abee meteorite is carried by cohenite and that "some kind of magnetic interaction might exist" between kamacite and cohenite. Rochette et al. [34] found for a lunar sample (Apollo basalt 14053) with high saturation remanence and susceptibility a low NRM unblocking temperature below 300 °C, which they suggested to be caused by cohenite or schreibersite. Similar unblocking temperatures of SIRM were found by Gattacceca et al. [22] in this rock, strengthening the case for cohenite. These phases can either be related to meteoritic contamination [35] or may occur as pristine phases in basalt [36]. Furthermore, the presence of mm-sized cohenite inclusions in the volcanic slags of Tolbachnik volcano (peninsula Kamchatka, Russia) suggests that cohenite can also have a magmatic origin [37] and probably is a significant carbon-bearing phase in the Earth mantle and core as suggested in earlier studies [16]. The results of our study support the idea that cohenite can be a good recorder of magnetic fields in planetary core material [2,20,38].

Acknowledgements

This work was funded by the priority program Planetary Magnetism of the German Research Foundation (DFG) (project KO1514/8: "Mineral magnetism of shocked ferrimagnetic minerals"). We are grateful to W. Luecke for kindly providing the meteorite sample. We thank D. Litvinov for conducting the EBSD investigations. B.R. thanks the members of the Institute for Rock Magnetism for a fellowship that was given in February 2016 and for the large support during the time of the stay. This article profited significantly from the constructive comments of an anonymous reviewer.

References

[1] E. Dos Santos, J. Gattacceca, P. Rochette, R.B. Scorzelli, G. Fillion, Magnetic hysteresis properties and 57Fe Mössbauer spectroscopy of iron and stony-iron meteorites: implications for mineralogy and thermal history, Phys. Earth Planet. Inter. 242 (2015) 50–64.
[2] N. Sugiura, D.W. Strangway, A paleomagnetic conglomerate test using the Abee E4 meteorite, Earth Planet. Sci. Lett. 62 (1983) 169–179.
[3] B.P. Weiss, J. Gattacceca, S. Stanley, P. Rochette, U.R. Christensen, Paleomagnetic records of meteorites and early planetesimal differentiation, Space Sci. Rev. 152 (2010) 341–390.
[4] W. Stankowski, A. Muszyński, K. Klimm, M. Schliestedt, Mineralogy of Morasko meteorite and the structure of the craters, Proc. Est. Acad. Sci. Geol. (2002) 227–240.
[5] M. Szurgot, K. Rozniakowski, T.W. Wojtatowicz, K. Polański, Investigation of microstructure and thermophysical properties of Morasko iron meteorites, Cryst. Res. Technol. 43 (2008) 921–930.
[6] W. Luecke, A. Kontny, U. Kramar, Geochemical zoning and magnetic mineralogy at Fe,Ni-alloy-troilite interfaces of three iron meteorites from Morasko, Coahuila II, and Mundrabilla, Meteorit. Planet. Sci. 49 (2014) 750–771.
[7] A.S. Pilski, J.T. Wasson, A. Muszyński, R. Kryza, Ł. Karwowski, M. Nowak, Low-Ir IAB irons from Morasko and other locations in central Europe: one fall, possibly distinct from IAB-MG, Meteorit. Planet. Sci. 48 (2013) 2531–2541.
[8] V. Geist, G. Wagner, G. Nolze, O. Moretzki, Investigations of the meteoritic mineral (Fe,Ni)3P, Cryst. Res. Technol. 40 (2005) 52–64.
[9] D.W. Mittlefehldt, T.J. McCoy, C.A. Goodrich, A. Kracher, Non-chondritic meteorites from asteroidal bodies, in: J.J.J. Papike (Ed.), Rev. Mineral. Planet. Mater. 36 (1), Mineralogical Society of America, 1998, pp. 1–195.
[10] J.T. Wasson, H. Huber, D.J. Malvin, Formation of IIAB iron meteorites, Geochim. Cosmochim. Acta 71 (2007) 760–781.
[11] D.Heymann, M.Lipschutz, B.Nielsen, E.Anders, Canyon Diablo meteorite: metallographic and mass spectrometric study of 56 fragments, J. Geophys. Reasearch. 71 (166AD) pp. 619–641
[12] A.E. Ringwood, Cohenite as a pressure indicator in iron meteorites, Geochem. Notes 26 (1958) 155–158.
[13] M. Lipschutz, E. Anders, Cohenite as a pressure indicator in iron meteorites-III Comments on a paper by Lipschutz and Anders, Geochim. Cosmochim. Acta 28 (1964) 699–711.
[14] R. Brett, Cohenite: its occurrence and a proposed origin, Geochim. Cosmochim. Acta 31 (1967) 143–159.
[15] J.A. Wood, Formation of chondritic refractory inclusions: the astrophysical setting, Geochim. Cosmochim. Acta 68 (2004) 4007–4021.
[16] B.J. Wood, Carbon in the core, Earth Planet. Sci. Lett. 117 (1993) 593–607.
[17] D.E. Jacob, A. Kronz, K.S. Viljoen, Cohenite, native iron and troilite inclusions in garnets from polycrystalline diamond aggregates, Contrib. Mineral. Pet. 146 (2004) 566–576.

[18] L. Gao, B. Chen, J. Wang, E.E. Alp, J. Zhao, M. Lerche, Pressure-induced magnetic transition and sound velocities of Fe3C: implications for carbon in the Earth's inner core, Geophys. Res. Lett. 35 (2008) 1–5.
[19] P. Rochette, G. Fillion, R. Ballou, F. Brunet, B. Oulladiaf, L. Hood, High pressure magnetic transition in pyrrhotite and impact demagnetization on Mars, Geophys. Res. Lett. 30 (13) (2003) 1683. http://dx.doi.org/10.1029/2003GL017359.
[20] N. Sugiura, D.-W. Strangway, The magnetic properties of the Abee meteorite: evidence for a strong magnetic field in the early solar system, Proc. Lunar Planet. Sci. 12B (1981) 1243–1256.
[21] I.G. Wood, L. Vočadlo, K.S. Knight, D.P. Dobson, W.G. Marshall, G.D. Price, Thermal expansion and crystal structure of cementite, Fe3C, between 4 and 600 K determined by time-of-flight neutron powder diffraction, J. Appl. Crystallogr. 37 (2004) 82–90.
[22] J. Gattacceca, M. Boustie, L. Hood, J.P. Cuq-Lelandais, M. Fuller, N.S. Bezaeva, Can the lunar crust be magnetized by shock: experimental groundtruth, Earth Planet. Sci. Lett. 299 (2010) 42–53.
[23] E. Appel, Stress anisotropy in Ti-rich titanomagnetites, Phys. Earth Planet. Inter. 46 (1987) 233–240.
[24] A. Hubert, R. Schäfer, Magnetic Domains, the Analysis of Magnetic Microstructures, Springer-Verlag Berlin Heidelberg, 1998 ISBN: 978-3-540-64108-7 (Print) 978-3-540-85054-0 (Online).
[25] P. Ramdohr, The opaque minerals in stony meteorites, J. Geodyn. 68 (1963) 2011–20136.
[26] L. Batista, U. Rabe, S. Hirsekorn, Determination of the easy axes of small ferromagnetic precipitates in a bulk material by combined magnetic force microscopy and electron backscatter diffraction techniques, Ultramicroscopy 146 (2014) 17–26.
[27] P. Blum, R. Pauthenet, Cem. Compt Rend. 237 (1953) 1501.
[28] M. Uehara, C.J. Van Der Beek, J. Gattacceca, V.A. Skidanov, Y. Quesnel, Advances in magneto-optical imaging applied to rock magnetism and paleomagnetism, Geochemistry, Geophys. Geosystems 11 (2010) 1–11.
[29] M. Uehara, J. Gattacceca, H. Leroux, D. Jacob, C.J. Van Der, Beek, magnetic microstructures of metal grains in equilibrated ordinary chondrites and implications for paleomagnetism of meteorites, Earth Planet. Sci. Lett. 306 (2011) 241–252.
[30] P. Dankers, N. Sugiura, The effects of annealing and concentration on the hysteresis properties of magnetite around the PSD-MD transition, Earth Planet. Sci. Lett. 56 (1981) 422–428.
[31] A.S. Keh, C.A. Johnson, Ferromagnetic domain structures in cementite, J. Appl. Phys. 34 (1963) 2670–2676.
[32] O. Perevertov, J. Thielsch, R. Schäfer, Effect of applied tensile stress on the hysteresis curve and magnetic domain structure of grain-oriented transverse Fe-3% Si steel, J. Magn. Magn. Mater. 385 (2015) 358–367.
[33] B.M. Moskowitz, S.L. Halgedahl, C.A. Lawson, Magnetic domains on unpolished and polished surfaces of titanium-rich titanomagnetite, J. Geophys. Res. 93 (1988) 3372–3386.
[34] P. Rochette, J. Gattacceca, A.V. Ivanov, M.A. Nazarov, N. Bezaeva, Magnetic properties of lunar materials: Meteorites, Luna and Apollo return samples., Earth Planet. Sci. Lett. 292 (2010) 383–391.
[35] I. Fleischer, C. Schröder, G. Klingelhöfer, J. Zipfel, R.V. Morris, J.W. Ashley, New insights into the mineralogy and weathering of the Meridiani Planum meteorite, Mars, Meteorit. Planet. Sci. 46 (2011) 21–34.
[36] A. El Goresy, P. Ramdohr, L.A. Taylor, The geochemistry of the opaque minerals in Apollo 14 crystalline rocks, Earth Planet. Sci. Lett. 13 (1971) 121–129.
[37] S.F. Glavatskih, M.E. Generalov, Cohenite in mineral associations from high-temperature gas evolutions of high-cracked Tolbachnik eruption (Kamchatka), Rep. Acad. Sci. 346 (1996) 796–799.
[38] B. Reznik, A. Kontny, Cohenite – a stable magnetic carrier in iron meteorites, IRM Q. 26 (2016) 2–3.